Device physics of polymer

Blom, Paul W. M.; Mihailetchi, Valentin D.; Koster, L. Jan Anton; Markov, Denis E.

Published in:
Advanced materials

DOI:
10.1002/adma.200601093

Publication date:
2007

DOI: 10.1002/adma.200601093

Device Physics of Polymer:Fullerene Bulk Heterojunction Solar Cells**

By *Paul W. M. Blom*,* *Valentin D. Mihailetchi*, *L. Jan Anton Koster*, and *Denis E. Markov*

Plastic solar cells bear the potential for large-scale power generation based on materials that provide the possibility of flexible, lightweight, inexpensive, efficient solar cells. Since the discovery of the photoinduced electron transfer from a conjugated polymer to fullerene molecules, followed by the introduction of the bulk heterojunction (BHJ) concept, this material combination has been extensively studied in organic solar cells, leading to several breakthroughs in efficiency, with a power conversion efficiency approaching 5 %. This article reviews the processes and limitations that govern device operation of polymer:fullerene BHJ solar cells, with respect to the charge-carrier transport and photogeneration mechanism. The transport of electrons/holes in the blend is a crucial parameter and must be controlled (e.g., by controlling the nanoscale morphology) and enhanced in order to allow fabrication of thicker films to maximize the absorption, without significant recombination losses. Concomitantly, a balanced transport of electrons and holes in the blend is needed to suppress the build-up of the space–charge that will significantly reduce the power conversion efficiency. Dissociation of electron–hole pairs at the donor/acceptor interface is an important process that limits the charge generation efficiency under normal operation condition. Based on these findings, there is a compromise between charge generation (light absorption) and open-circuit voltage (V_{OC}) when attempting to reduce the bandgap of the polymer (or fullerene). Therefore, an increase in V_{OC} of polymer:fullerene cells, for example by raising the lowest unoccupied molecular orbital level of the fullerene, will benefit cell performance as both fill factor and short-circuit current increase simultaneously.

1. Introduction

Harvesting energy directly from the sunlight using photovoltaic (PV) technology is being widely recognized as an essential component of future global energy production. Provided that PV devices can be made truly economically competitive with fossil fuels and other emerging renewable energy technologies, large-scale manufacturing of these devices offers a sustainable energy source that can supply a significant fraction of our daily energy needs. Photovoltaic cells have become extensively studied since the 1950s when the first crystalline silicon solar cell, which had an efficiency of 6 %, was developed at Bell Laboratories.[1] Since then, the efficiency has reached 24 % for crystalline Si solar cells,[2] which is already close to the theoretical predicted upper limit

[*] Prof. P. W. M. Blom, Dr. V. D. Mihailetchi, Dr. L. J. A. Koster, Dr. D. E. Markov
Molecular Electronics
Zernike Institute for Advanced Materials
University of Groningen
Nijenborgh 4, 9747 AG Groningen (The Netherlands)
E-mail: p.w.m.blom@rug.nl

[**] The authors especially acknowledge the contributions of Kees Hummelen, Bert de Boer, Jur Wildeman, Minte Mulder, Alex Sieval, and Edsger Smits to this work. These investigations were financially supported by the Dutch Ministries of EZ, O&W, and VROM through the EET program (EETK97115). The work of L.J.A.K forms part of the research program of the Dutch Polymer Institute (# 323). The work of D.E.M is part of the research program of the Stichting voor Fundamenteel Onderzoek der Materie (FOM, financially supported by the Nederlandse Organisatie voor Wetenschappelijk Onderzoek (NWO)).

of 30 %.[3,4] Practically all conventional inorganic solar cells incorporate a semiconductor that is doped to form a p-n junction across which the photovoltage is generated. The p side contains an excess of the positive charges (holes), and the n side contains an excess of the negative charges (electrons). In the region near the junction, an electric field is formed and the electrons and holes, which are generated by light absorption in the bulk Si, diffuse to this junction where they are directed by the electric field towards the proper electrode. Over the years, solar cells have been made from many other semiconductor materials with various device configuration such as single-crystal, polycrystalline, and amorphous thin-film structures. Organic materials bear the potential to develop a long-term technology that is economically viable for large-scale power generation based on environmentally safe materials with unlimited availability. Organic semiconductors are a less expensive alternative to inorganic semiconductors like Si. Compared to Si, they can have extremely high optical absorption coefficients that offer the possibility for the production of very thin solar cells. Additional attractive features of organic PVs are the possibilities for thin flexible devices which can be fabricated using high-throughput, low-temperature approaches that employ well established printing techniques in a roll-to-roll process.[5,6] This possibility of using flexible plastic substrates in an easily scalable high-speed printing process can reduce the balance of system cost for organic PVs, resulting in a shorter energetic pay-back time.

The first investigation of an organic PV cell came as early as 1959, when an anthracene single crystal was studied. The cell exhibited a photovoltage of 200 mV with an extremely low efficiency.[7] Since then, many years of research has shown that the typical power conversion efficiency of PV devices based on single (or homojunction) organic materials will remain below 0.1 %, making them unsuitable for any possible application. Primarily, this is due to the fact that absorption of light in organic materials almost always results in the production of a mobile excited state (referred to as exciton), rather than free electron–hole (e–h) pairs as produced in inorganic solar cells. This occurs because in organic materials the weak intermolecular forces localize the exciton on the molecules. Combined with a low dielectric constant (typically 2–4) compared to inorganic semiconductors, a much higher energy input than the thermal energy (kT) is required to dissociate these excitons.[8–10] The electric field provided by the asymmetrical work functions of the electrodes is not sufficient to break up these photogenerated excitons. Instead, the excitons diffuse within the organic layer until they reach the electrode, where they may dissociate to supply separate charges, or recombine. Since the exciton diffusion lengths are typically 1–10 nm,[11–15] much shorter than the device thicknesses, exciton diffusion limits charge-carrier generation in these devices because most of them are lost through recombination. Photogeneration is therefore a function of the available mechanisms for excitons dissociation. A major breakthrough in cell performance came in 1986 when Tang discovered that much higher efficiencies (about 1 %) can be attained when an electron donor (D) and an electron acceptor (A) are brought together in one cell.[16] This heterojunction concept is at the heart of all three types of organic PV cells that currently exist: dye-sensitized solar cells;[17–19] planar organic semiconductor cells;[16,20–22] and high surface area, or bulk heterojunction (BHJ) cells.[5,23–25] The idea behind a heterojunction is to use two materials with different electron affinities and ionization potentials. At the interface, the resulting potentials are strong and may favor exciton dissociation: the electron will be accepted by the material with the larger electron affinity and the hole will be accepted by the material with the lower ionization potential, provided that the difference in potential energy is larger than the exciton binding energy. In the planar heterojunction, or "bi-layer" device, the organic D/A interface separates excitons much more efficient than an organic/metal interface in the single layer device. In this device the excitons should be formed within the diffusion length of the interface. Otherwise, the excitons will decay, yielding, e.g., luminescence instead of a contribution to the photocurrent. Since the exciton diffusion lengths in organic materials are much shorter than the absorption depth of the film, this limits the width of effective light-harvesting layer. A revolutionary development in organic PVs came in the mid 1990s with the introduction of the dispersive (or bulk) heterojunction, where the donor and acceptor material are blended together. If the length scale of the blend is similar to the exciton diffusion length, the exciton decay processes is dramatically reduced since in the proximity of every generated exciton there is an

Paul W. M. Blom received his Ir. degree (Physics) in 1988 and his Ph.D. degree in 1992, from the Technical University Eindhoven, Eindhoven, The Netherlands. Joining Philips Research Laboratories in 1992 he was engaged in the electrical characterization of various oxidic thin-film devices, the electro-optical properties of polymer light-emitting diodes, and the field of rewritable optical storage. In May 2000 he was appointed as a Full Professor at the University of Groningen, where he leads a group in the field of electrical and optical properties of organic semiconducting devices. At present the main focus is on the device physics of polymeric light-emitting diodes, transistors, solar cells, and molecular electronics.

ADVANCED MATERIALS

interface with an acceptor where fast dissociation takes place. Hence, charge generation takes place everywhere in the active layer. Provided that continuous pathways exist in each material from the interface to the respective electrodes, the photon-to-electron conversion efficiency and, hence, the photosensitivity is dramatically increased.

One class of organic materials used as photoactive layer in bulk heterojunction PV cells that have received considerable attention in the last few years are semiconducting polymers and molecules. They combine the optoelectronic properties of conventional semiconductors with the excellent mechanical and processing properties of "plastic" materials. Additionally, they possess an unprecedented flexibility in the synthesis, allowing for alteration of a wide range of properties, such as bandgap, molecular orbital energy level, wetting and structural properties, as well as doping. This ability to design and synthesize polymers and molecules that can be cast from solution using wet-processing techniques such as spin-coating, ink-jet printing, and screen printing represents an enormous attractive route for cheap production of large-area PV cells that can be applied to systems that require flexible substrates. Because luminescence quenching[26] and ultrafast photoinduced electron transfer[27] from a conjugated polymer (as donor) to buckminsterfullerene (C60) or its derivatives (as acceptor) had already been observed in 1992, this material combination has been extensively studied in bulk heterojunction PV cells. In 1995 Yu et al.[24] fabricated the first fully organic BHJ cell based on a mixture of soluble *p*-phenylene vinylene (PPV) derivative with a fullerene acceptor. In 2001, Shaheen et al.[28] obtained the first truly promising results for BHJ solar cells when mixing the conjugated polymer poly(2-methoxy-5-(3′,7′-dimethyl-octyloxy)-*p*-phenylene vinylene) (MDMO-PPV) and methanofullerene [6,6]-phenyl C_{61}-butyric acid methyl ester (PCBM) in a 20:80 wt % and optimizing the nanoscale morphology of the film, yielding a power conversion efficiency of 2.5 %. Recently, the attention has been shifted towards polymer:fullerene (like PCBM) BHJ solar cells based on polythiophene derivatives as absorbing and electron donating material.[29–33] By optimizing the processing conditions, efficiencies in excess of 4 % have been reported for this materials system.[34–36]

The fundamental physical processes in a BHJ device are schematically represented in an energetic diagram as depicted in Figure 1. Sunlight photons which are absorbed inside the device excite the donor (1), leading to the creation of excitons in the conjugated polymer. The created excitons start to diffuse (3) within the donor phase and if they encounter the interface with the acceptor then a fast dissociation takes place (4) leading to charge separation.[27,37] The resulting metastable electron–hole pairs across the D/A interface may still be Coulombically bound and an electric field is needed to separate them into free charges.[38,39] Therefore, at typical operation conditions, the photon-to-free-electron conversion efficiency is not maximal. Subsequently, the separated free electrons (holes) are transported (5) with the aid of the internal electric field, caused by the use of electrodes with different work functions, towards the cathode (anode) where they are collected by the electrodes (6) and driven into the external circuit. However, the excitons can decay (2), yielding, e.g., luminescence, if they are generated too far from the interface. Thus, the excitons should be formed within the diffusion length of the interface, being an upper limit for the size of the conjugated polymer phase in the BHJ. In this review we will discuss these subsequent fundamental processes using a MDMO-PPV:PCBM (1:4 wt %) as a model system and evaluate their role for solar cell performance.

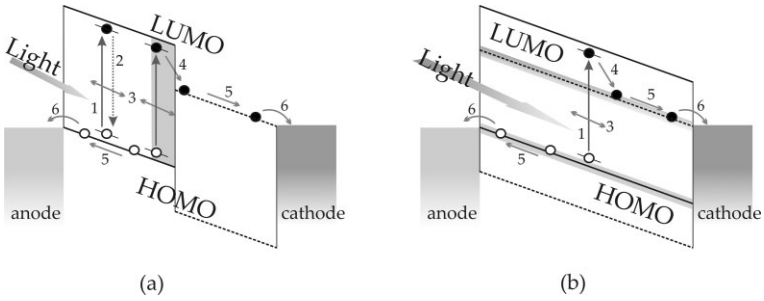

Figure 1. Schematic band diagram of a) a bilayer device and b) a bulk heterojunction. The numbers refer to the operation processes explained in the text. The dashed line represents the energy levels of the acceptor, while the full lines indicate the energy level of the donor in the PV cell. HOMO: highest occupied molecular orbital; LUMO: lowest unoccupied molecular orbital.

2. Physical Processes in Polymer:Fullerene Bulk Heterojunction Solar Cells

2.1. Creation of Excitons

To reach a high efficiency, the active layer of a solar cell should capture a large fraction of the incoming sun light. Because of the high absorption coefficient (ca. 10^5 cm^{-1}), conjugated polymers absorb light very efficiently at the maximum of their absorption spectrum. As a result a layer thickness of only a few hundred nanometer is required to absorb all the light at their peak wavelength absorption. As a comparison to silicon based solar cells, active layer thicknesses of hundreds of micrometers are required since silicon is an indirect semiconductor. However, because the absorption bands of conjugated polymers are relatively narrow compared to inorganic semiconductors, the performance of solar cells based on polymers is poor compared to inorganic solar cells. In an organic solar cell, only a small region of the solar spectrum is covered. For example, a bandgap of 1.1 eV is required to cover 77 % of the AM1.5 (air mass) solar photon flux (assuming complete absorption of the solar emission intensity by the material), whereas most solution processable semiconducting polymers (PPVs, poly(3-hexylthiophene) (P3HT)) have bandgaps larger than 1.9 eV, which covers only 30 % of the AM1.5 solar

photon flux (assuming complete absorption of the solar emission intensity by the material). In addition, as will be discussed later, because of the low charge-carrier mobilities of most polymers, the thickness of the active layer is limited to ca. 100 nm, which, in turn, results in an absorption of only ca. 60 % of the incident light at the absorption maximum (without back reflection of the electrode).

When photons with energy beyond the absorption edge are incident on a semiconducting specimen of the polymer, an electron and hole with opposite spin are created, bound by their Coulomb attraction in a singlet exciton state. Because coupling between neighboring molecules in molecular solids is low, the molecular excitations are localized and there is no band to band transition, unlike in inorganic semiconductors. Concomitantly, the relative dielectric constant of the order of 3, as compared to 10 in inorganic semiconductors, results in strongly bound Frenkel-like localized excitons. Hence, exciton effects are important at room temperature, in contrast to inorganic Wannier-type excitons with a binding energy of about kT at room temperature. An important question is the magnitude of the binding energy (EB) of the exciton in conjugated polymers. The disorder present in conjugated polymers prevents the exciton binding energy from being a well-defined material quantity. The activation energy of photoconductivity in PPV-type systems cannot be used to characterize the exciton binding energy because extrinsic effects usually prevail in charge-carrier formation from the singlet exciton S1 state. Although it has been suggested that EB is of the order of, or less than kT,[40] there is a large amount of experimental evidence for a much stronger binding. A Monte Carlo simulation study has been conducted to model bimolecular charge recombination, treated as a random walk of a pair of charges in an energetically roughened landscape, with superimposed long-range coulomb interactions.[41] This analysis has demonstrated that the effective recombination cross-section of a charge carrier decreases sharply as EB decreases. Under the condition $EB \leq$ kT, the probability for recombination of a pair of charge carriers is almost two orders of magnitude less than the recombination required to explain the performance of polymer-based light-emitting diodes (LEDs). On the other hand $EB > 0.2$ eV granted a sufficient recombination cross section. The exciton binding energy has been experimentally derived from studies of the photovoltaic response of PPV based diodes, leading to an exciton binding energy of approximately 0.4 eV.[10] One of the most convincing quantitative assessments of the exciton binding energy magnitude is provided by studying the photoluminescence quenching resulting from an electric field.[42,43] The dissociation of an excited singlet state of a conjugated polymer requires field-assisted transfer of the constituent charges to a neighboring chain or chain segment. In a first order approximation, this would occur if the gain in electrostatic energy, $eE\Delta z$, where e is the electric charge, E the internal electric field, and Δz the distance between the charges, compensates for the energy expense for the charge transfer in zero field. Using $\Delta z = 10$ Å and $E = 2 \times 10^6$ V cm^{-1}, leads to a $eE\Delta z = 0.2$ eV. Indeed, considerable steady-state photoluminescence (PL) quenching has been observed for films of poly-(phenyl-*p*-phenylene vinylene)/polycarbonate (PPPV/PC) blends upon application of an electric field of this order of magnitude. Monte Carlo simulations of the field dependence of PL quenching give a good fit to experimental data for values of $EB = 0.4 \pm 0.1$ eV. Besides field-assisted exciton dissociation, these simulations take into account radiative decay, energy relaxation within an inhomogeneously broadened density of states, and exciton capture by nonradiative traps.

2.2. Diffusion of Excitons in Conjugated Polymers

Because of the high exciton binding energy in conjugated polymers, the thermal energy at room temperature is not sufficient to dissociate a photogenerated exciton (typical binding energy of 0.4 eV) into free charge carriers. Consequently, the configuration and operation principle of photovoltaic devices based on organic semiconductors differ significantly from those based on inorganic materials. Typically, in organic solar cells an efficient electron acceptor is used in order to dissociate the strongly bound exciton into free charge carriers.[16] The exciton diffusion length L_D, which characterizes the effective width of the active area of the polymer film at the acceptor interface, has been reported to be 5–8 nm in PPV-based conjugated polymers.[12,14,15] Because the exciton diffusion length in a conjugated polymer is typically less than the photon absorption length (ca. 100 nm), the efficiency of a bilayer cell is limited by the number of photons that can be absorbed within the effective exciton diffusion range at the polymer/electron acceptor interface. To circumvent the problem of limited exciton diffusion length in conjugated polymers, the bulk heterojunction PV cell architecture has been developed by simply blending the polymer with a soluble electron acceptor.[23,44] In the ideal case, the characteristic (reduced) size of the polymer phase in the active layer of the cell grants that all excitons are formed within the diffusion distance from an electron acceptor interface. As a result, such an interpenetrating donor:acceptor network allows photon absorption improvement by a simple increase of the active-layer thickness, thereby maintaining an efficient dissociation of excitons. Exciton diffusion is therefore a beneficial process for polymer-based PV cells because it governs the transfer of the photoexcitation energy towards the electron donor/acceptor interface, where charge carriers are formed. Improvement of the exciton diffusion allows for bigger sized polymer domains leading to an enhanced absorption and solar cell performance.

The exciton diffusion lengths in various conjugated polymers reported in the literature show a large variation, ranging from 5 to 20 nm.[12,45–49] Most of these studies make use of a bilayer model system, comprising of an evaporated C60 layer in combination with a conjugated polymer spin-coated from the solution. From photocurrent measurements on the precursor poly(*p*-phenylene vinylene) (PPV)/C60 photovoltaic devices an exciton diffusion length of 7 ± 1 nm has been de-

ADVANCED MATERIALS

duced.[12] In this work it was stressed that a precursor PPV with a relatively high glass transition temperature was used in order to avoid C60 interdiffusion into the relatively soft PPV. Comparatively, from photocurrent spectra of the same material combination, an exciton diffusion length of 12±3 nm has been derived.[47] A more direct way, which decouples the device performance (photocurrent) from the exciton diffusion, is to study the quenching of the photoluminescence from polymer/fullerene bi-layer heterostructures. In this approach, the photogenerated exciton population is directly probed. The change in the photoluminescence with varying polymer layer thickness in a heterostructure directly reflects the change in exciton population due to their diffusion and subsequent charge transfer at the interface. The quenching of the PL of a ladder-type conjugated polymer that was spin-coated on top of a C60-fullerene-based self-assembled monolayer has been measured, and an exciton diffusion length of 14 nm has been deduced from these measurements.[46] Furthermore, from the PL quenching of heterojunctions consisting of polythiophene and evaporated C60, an exciton diffusion length of 5 nm has been obtained.[45]

A major problem in the determination of L_D using luminescence quenching is the intermixing of the evaporated C60 molecules with the soft polymer layer, which obscures the intrinsic exciton diffusion process. Using photoelectron spectroscopy and X-ray absorption, it has been demonstrated that at room temperature evaporated C60 diffuses into spin-cast poly(3-octylthiophene) (P3OT) layer after deposition.[49] The time-scale of this indiffusion process of C60 into P3OT typically amounts to thirty minutes. In a recent study we used an alternative approach: instead of an evaporated C60 layer as an acceptor we used a polymerizable fullerene layer (poly(F2D)).[14] After thermopolymerization the fullerenes are immobilized, preventing the electron acceptor molecules to diffuse into the polymer, and the polyfullerene layer is insoluble in common solvents. This makes this polyfullerene layer an ideal model system to study exciton diffusion in heterojunctions with any soluble conjugated polymers which are interesting for solar cells. It can be shown that in such a sharply defined bilayer system the exciton quenching yield Q as a function of polymer film thickness L is given by

$$Q = \frac{(a^2L_D^2 + aL_D \tanh(L/L_D))\exp(-aL) - a^2L_D^2(\cosh(L/L_D))^{-1}}{(1 - a^2L_D^2)(1 - \exp(-aL))} \quad (1)$$

where a is the absorption coefficient and L_D is the exciton diffusion length, being the only fit parameter in this model. In Figure 2 the luminescence quenching is plotted for a bilayer device consisting of the random copolymer of poly(2-methoxy-5-(3′,7′-dimethyloctyloxy)-*p*-phenylene vinylene) and poly[4′-(3,7-dimethyloctyloxy)-1,1′-biphenylene-2,5-vinylene] (NRS-PPV), which is a soluble PPV-derivative, and the polyfullerene. Attributing this quenching to the diffusion of excitons towards the well-defined polymer/fullerene interface the experimental data are well described by an exciton diffusion length of 5±1 nm (Fig. 2, solid line). This is in agreement with earlier reported results, where C60 indiffusion was prevented as much as possible by choosing a "hard" precursor PPV.[12] The quenching effects are most pronounced in films with thicknesses smaller than 30 nm. In this thickness regime, interference effects into the photogeneration profile can be neglected. The experiments have been extended to other PPV-based derivatives, including MDMO-PPV that is used in solar cells.[15] Because of chemical modifications, the various PPV derivatives differ in charge-carrier mobility by three orders of magnitude as a result of a reduced energetic disorder. From the photoluminescence decay curves of PPV/fullerene heterostructures, the exciton diffusion coefficient was found to increase by only one order of magnitude with decreasing disorder. However, the increase in the diffusion coefficient is compensated by a decrease of the exciton lifetime, leading to an exciton diffusion length of 5–6 nm for all the PPV derivatives studied. Furthermore, it should be noted that besides exciton diffusion and subsequent electron transfer, resonant energy transfer towards C60-based acceptors can also play a role. Recent theoretical[50] and experimental studies[51] have revealed that under certain circumstances the rate of both mechanisms can compete, which would require a reinterpretation of the luminescence quenching measurements. How far this applies to the PPV:PCBM blends as used in BHJ solar cells is under discussion.

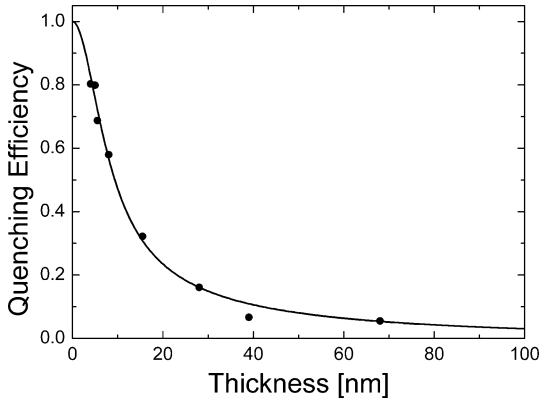

Figure 2. The relative luminescence quenching in NRS-PPV/poly(F2D) heterostructures for different polymer film thicknesses. A fit of these data with Equation 1 (solid lines) using an exciton diffusion length of 5 nm is shown.

2.3. Dissociation of Charge Carriers at the Donor/Acceptor Interface

Organic semiconductors are characterized by low relative dielectric constants, typically ranging from 2 to 4. As a result, for a photogenerated electron and hole at the donor/acceptor interface the Coulomb binding energy can be very strong. For example, for a spatial separation of 1 nm between the elec-

tron–hole pair the Coulomb binding typically amounts to ca. 0.5 eV. As a result, the bound electron–hole pair either recombines or dissociates into free charge carriers when the carriers are able to escape their mutual Coulomb attraction. In molecular solids it is generally accepted that the photogeneration of charge carriers results from field- and temperature-assisted dissociation of singlet excitons.[52–55] The field dependence of the charge generation process has been consistently described using models based on Onsager theory.[56] In this theory, the dissociation of a bound electron–hole pair is described as a diffusive Brownian motion of the charges within their Coulombic potential modified by an applied electric field. The dissociation efficiency depends on the initial separation distance of the charge carriers and the strength of the applied field. For conjugated polymers the situation is less clear. Field-assisted quenching of photoluminescence demonstrated that a strong field is indeed required to dissociate the neutral excitonic state.[43] However, the measured dissociation of excitons does not reveal whether free carriers or bound charge-carrier pairs are formed upon breaking of the exciton. By combining exciton quenching with photoluminescence and photocurrent measurements, it was found that for a ladder-type polymer, the generation of free charges is a two-step process: In the first step Coulombically bound geminate electron–hole pairs are formed, and secondly the pairs are dissociated into free carriers.[57] In contrast to earlier assumptions, the electric field mainly assists in the formation of the bound pairs and not in their dissociation.

An important question is whether these bound pairs are also present in donor/acceptor systems that are relevant for solar cells as bilayers and bulk heterojunctions. A strongly bound electron–hole pair seems in direct contradiction with the high internal quantum yields that are achieved in polymer/fullerene blends. It has been proposed that the exciton directly dissociates into free charge carriers because the excess photon energy after exciton dissociation is used to separate the bound pair at the interface.[58] Alternatively, it has been pointed out that the excess energy of the hot carriers formed directly after charge transfer governs the initial separation distance between the bound electron and hole, and thus the dissociation efficiency.[59] In bilayer devices, the interface also plays an important role since the orientation of the electric dipole favors separation perpendicular to the interface, in alignment with the field in the solar cells.[59] Furthermore, a large mobility difference is expected to favor dissociation as well.[59,60] Arkhipov et al. have pointed out that the interface might play an additional important role.[61] A dipole layer at the interface, due to partial charge transfer prior to photoexcitation, prevents back transfer of the hole and reduces the probability of recombination of the bound pair. In a recent study, two-pulse femtosecond spectroscopy with photocurrent detection was used to optically detect the presence of bound electron–hole pairs in polymer:fullerene blends.[62] Coulombically bound charge carrier pairs were found in a ladder-type polymer, but not in MDMO-PPV:fullerene blends. However, these blends were processed from toluene, in which MDMO-PPV is known to form relatively big clusters, leading to inefficient solar cells.[28] Whether these measurements are therefore representative of blends processed from chlorobenzene, which do yield solar cells that have an efficiency of 2.5 %, is not clear.

In the case of an ideal solar cell, meaning no recombination and space–charge formation, the photocurrent can also be a direct measure of the photogeneration of free charge carriers. In that case the internal field in the device is given by $E = (V_{oc} - V)/L$, where V is the applied voltage, V_{oc} is the open-circuit voltage, and L is the thickness of the active layer. The photocurrent for holes is then given by $J_{ph} = ep\mu E$, where μ is the hole mobility and p is the density of photogenerated holes, which at steady state is given by their lifetime and generation rate (G), $p = \tau G$. At long lifetimes (little or no recombination), all photogenerated charge carriers leave the device before recombining, and their lifetime becomes equal to the transit time, $\tau_t = L^2/\mu V$. From this it follows directly[63] that the hole photocurrent through the external circuit is simply

$$J_{ph} = eGL \tag{2}$$

An identical result can be obtained for electrons. Thus, for a constant generation rate G of electron–hole pairs, J_{ph} is independent of V. As a result, in this ideal case, the photocurrent given by Equation 2 is independent of the mobility of either electrons or holes and a direct measure of G, because for none or very weak recombination, the carrier lifetime will always exceed the transit time. The presence of bound charge carriers can be monitored using photoinduced absorption spectroscopy. It has recently been demonstrated that the dynamics of the charge-carrier recombination extends all the way into the millisecond regime.[58,64–66] With a typical hole-transit time at short-circuit of only a microsecond (see following section) it is expected that at high reverse bias, where the transit time is further shortened, most of the generated charges leave the device without recombining and Equation 2 applies. However, Hughes and Sokel[67] pointed out that Equation 2 is incorrect at low bias voltages because diffusion currents have been neglected. Using the same approximation as in Equation 2 but including diffusion, the photocurrent is given by

$$J_{ph} = eGL\left[\frac{\exp(eV/kT)+1}{\exp(eV/kT)-1} - \frac{2kT}{eV}\right] \tag{3}$$

where eGL is the saturated photocurrent from Equation 2, V the applied voltage, k the Boltzmann constant and T is the temperature. In Figure 3, a reverse voltage sweep from 1 V to –10 V was applied under illumination (800 W m^{-2}, in an inert (N_2) atmosphere) and the photocurrent density (J_L) was recorded for a temperature range of 210–295 K. In order to determine the effective photocurrent, the current density in the dark (J_D) was also recorded. The effective experimental photocurrent is given by $J_{ph} = J_L - J_D$. In Figure 3, J_{ph} is plotted on a double logarithmic scale against the effective voltage across the device, given by $V_0 - V$. The effective voltage V_0 is defined as the voltage where $J_L = J_D$ and is slightly larger than V_{OC}. The solutions of Equations 2 and 3 are shown sche-

ADVANCED MATERIALS

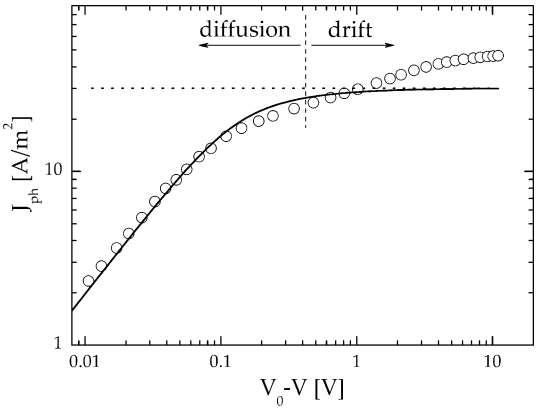

Figure 3. Room-temperature current density–voltage (*J–V*) characteristics of an MDMO-PPV:PCBM (20:80 wt %) device as a function of effective applied voltage ($V_0 - V$) (symbols). The solid line represents the calculated photocurrent from Equation 3 using $G = 1.46 \times 10^{27}$ e–h pairs m^{-3} s^{-1}, whereas the dotted line represents the drift current calculated from Equation 2 using the same *G*.

matically in Figure 3 together with the experimental data. Using a G of 1.46×10^{27} e–h pairs m^{-3} s^{-1}, Equation 3 fits the experimental data very well at low effective voltage ($V_0 - V < 0.1$ V), indicating that diffusion plays an important role in the experimental photocurrent. At higher reverse voltage ($V_c - V > 1$ V) the photocurrent increases further with increasing voltage. From Figure 3, it appears that for effective voltages exceeding 1 V the experimental photocurrent does not saturate at eGL but gradually increases. However, an important process that has not been taken into account in Equation 2 is that not all the photogenerated bound electron–hole pairs (represented by G_{MAX}) dissociate into free charge carriers. Only a certain fraction of G_{MAX} is dissociated into free charge carriers, depending on the field and the temperature, and therefore contributes to the photocurrent (eGL). Consequently, the generation rate G of free charge carriers can be described by

$$G(T,E) = G_{MAX} P(T,E) \tag{4}$$

where $P(T,E)$ is the probability of charge separation at the donor/acceptor interface. As stated above, the photogeneration of free charge carriers in low-mobility materials can be explained by the geminate recombination theory of Onsager.[56] An important addition to the theory has been made by Braun,[38] who stressed the importance of the fact that the bound electron–hole pair (or charge-transfer state) has a finite lifetime. The bound electron–hole pair, formed after dissociation of an exciton at the donor–acceptor interface, can either decay to its ground state with a rate constant k_F or separate into free carriers with an electric-field-dependent rate constant $k_D(E)$. Once separated, the charge carriers can again form a bound pair with a rate constant k_R. Consequently, free carriers which are captured into bound pairs may dissociate again during the lifetime of the bound pair. Therefore, long lived charge transfer states act as a precursor for free charge carriers. In Braun's model, the probability that a bound polaron pair dissociates into free charge carries at a given electric field E and temperature T is given by

$$P(T,E) = \frac{k_D(E)}{k_D(E) + k_F} \tag{5}$$

Using the Onsager theory for field-dependent dissociation rate-constants of weak electrolytes[56] for $k_D(E)$, Langevin recombination of free electrons and holes, and a Gaussian distribution of donor–acceptor distances, the generation rate of free electrons and holes in blends of MDMO-PPV:PCBM for any temperature and electric field can be calculated.[68] It should be noted that this calculation involves only two adjustable parameters: the initial separation of e–h pairs, a, and the ground state recombination rate k_F, as all the other parameters were experimentally determined. Figure 4 (solid lines) shows the calculated photocurrent (J_{ph}) from Equation 2 as a function of temperature, including the calculated field-dependent generation rate $G(T,E)$. Using a separation distance

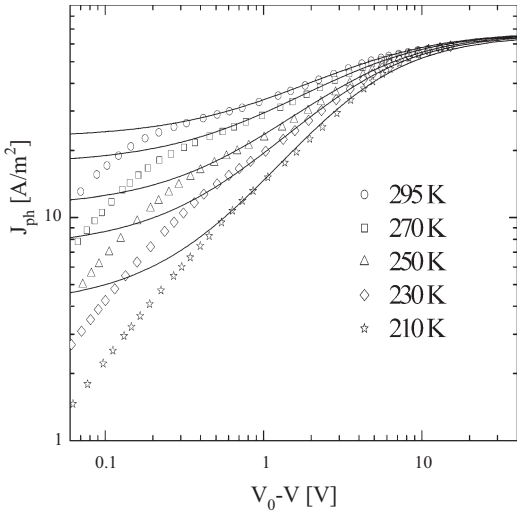

Figure 4. Temperature dependence of the photocurrent (symbols) versus effective applied voltage ($V_0 - V$) for a device of 95 nm thickness. The solid line represents the calculated photocurrent from Equation 2 using the field- and temperature-dependent generation rate $G(T,E)$.

$a = 1.4$ nm, and a room-temperature recombination lifetime $k_F^{-1} = 7$ μs, the calculations consistently describe the field- and temperature dependence of the experimental data in the saturation regime ($V_{oc} - V > 1$ V). At low effective voltages (< 1 V) $G(T,E)$ tends to saturate and the calculated values, together with Equation 2, predict the dependence of the photocurrent on temperature in this low-voltage regime. At high effective voltages (typically 10 V) the photocurrent saturates and becomes field and temperature independent. At these voltages all bound e–h pairs are separated and the maximum photocurrent $J_{SAT} = e\, G_{MAX}\, L$ is reached. It should be noted

that this high-voltage regime can be obscured by dark injection currents. However, by using a PEDOT electrode with lower conductivity this effect can be suppressed. By comparing the photocurrent with the experimentally observed J_{SAT} the dissociation efficiency can be read directly from Figure 4. Under short-circuit conditions ($V = 0$) only 60 % of the bound e–h pairs dissociate. This incomplete dissociation of generated bound electron–hole pairs under operating conditions is therefore a main loss mechanism in solar cells based on PPV/PCBM blends.

2.4. Charge Transport in Polymer:Fullerene Blends

After photoinduced electron transfer at the donor/acceptor interface and subsequent dissociation, the electrons are localized in the PCBM phase whereas the holes remain in the PPV polymer chains. Subsequently, the free electrons and holes must be transported via percolated PCBM and PPV pathways towards the electrodes to produce the photocurrent. Therefore, the electron transport in PCBM and hole transport in PPV are crucial for the understanding of the optoelectronic properties of BHJ solar cells. For pure PCBM[69] the electron mobility ($\mu_e = 2.0 \times 10^{-7}$ $m^2 V^{-1} s^{-1}$) was found to be 4000 times higher than the hole mobility in pure MDMO-PPV[70] ($\mu_h = 5.0 \times 10^{-11}$ $m^2 V^{-1} s^{-1}$). An important question is whether these mobilities are modified when the materials are blended as in the active layer of a solar cell. In one of the first studies using field-effect measurements, an increase of the hole mobility was observed in the PPV:PCBM blends.[71] However, it should be noted that in field-effect transistors the hole mobility of pristine MDMO-PPV is also three orders of magnitude larger compared to the hole mobility in light-emitting diodes or solar cells.[72] This enhancement is a result of the dependence of the mobility on charge carrier density, which is orders of magnitude higher in a transistor than in a solar cell.[72] Therefore, the values obtained for the electron and hole mobility can not be quantitatively applied to other device configurations such as light-emitting diodes or solar cells. Also, from time-of-flight photocurrent measurements,[73,74] an enhancement of the hole mobility was observed that was also dependent on the light intensity used. The dependence of the mobility on the carrier density might also be responsible for this effect. Recently, we have found that the hole mobility in a 20:80 wt % MDMO-PPV:PCBM blend is enhanced by more than two orders of magnitude as compared to the pure polymer value using space-charge-limited current (SCLC) measurements.[75] As a result, the difference between electron- and hole mobility is reduced to only a factor of ca. 10, resulting in more balanced transport. We also confirmed this mobility enhancement by transient methods including transient electroluminescence and impedance spectroscopy. The fact that the SCLC and transient measurements give the same mobility also shows that the hole transport is nondispersive in these blends. Although the enhancement of the hole mobility by blending with PCBM is not yet fully understood, it clearly indicates that hole- and electron mobility must be directly measured in the blend as used in the operational device

In order to measure the SCLC of only one type of charge carrier in a blend, the other one must be suppressed by a large injection barrier, resulting in an electron- or hole-only device. This approach has been successfully used to measure the hole-only SCLC in a 20:80 wt % MDMO-PPV:PCBM blend when Pd is employed as a top electrode.[75] For measurement of the electron current, the bottom contact must have a low work function to suppress hole injection into the MDMO-PPV. In order to obtain a low work function electrode that does not interact with the solvent during spin coating, we modified the work function of the noble metal Ag by using polar molecules that can self-assemble on the metal and form a highly ordered (2D) thin layer with a dipole in the desired direction.[76,77] Using a self-assembled monolayer (SAM) of hexadecanethiol on a flat 20 nm layer of Ag lowered its work function by 0.6 eV to 3.8 eV, as measured by the Kelvin probe.[77] From the work function of the Ag/SAM and highest occupied molecular orbital (HOMO) level of PPV a hole injection barrier of ca. 1.3 eV is expected. This large injection barrier suppresses the hole current very efficiently, such that, even in a blend with a low PCBM ratio and reduced electron transport the current is still electron dominated. Thus, electron- and hole-only devices are constructed that enable us to measure the SCLCs of electrons or holes separately in MDMO-PPV:PCBM blends with various composition.[78] The resulting mobilities from the single carrier SCLCs in MDMO-PPV:PCBM BHJ devices are presented as a function of wt % PCBM in Figure 5. A gradual increase of electron mobility with increasing fullerene concentration is observed from 33 to 80 wt %, followed by saturation to the value of pure PCBM (2×10^{-7} $m^2 V^{-1} s^{-1}$).[69] It is observed that this saturation does not coincide with the start of the phase separation (ca. 67 wt %),[79] but rather at the maximum device performance. Surprisingly, the hole mobility shows a similar behav-

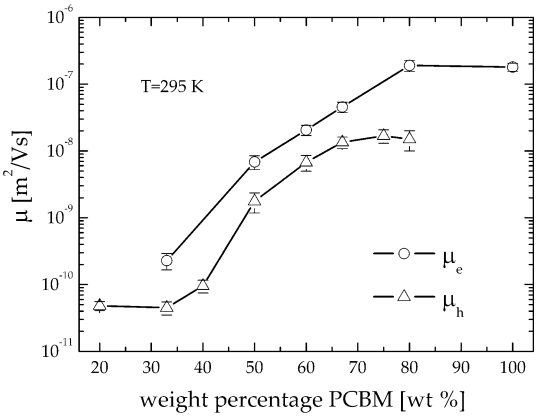

Figure 5. Electron μ_e and hole μ_h zero-field mobilities in blends of MDMO-PPV:PCBM as a function of PCBM weight percentage, at room temperature (295 K). The mobilities were calculated from SCL currents [78]. The electron mobility for 100 wt % PCBM was taken from the literature [69].

ADVANCED MATERIALS

ior as a function of fullerene concentration. A similar behavior has recently being reported using time-of-flight (TOF) measurements.[80]

Intuitively, one would expect that "dilution" of the PPV with PCBM would lead to a reduction of the hole transport properties, for example due to a reduced percolation pathway. However, it is observed that from 40 to 80 wt % PCBM the hole mobility increases by more than two orders of magnitude from its pure polymer value (5×10^{-11} $m^2 V^{-1} s^{-1}$) to approximately 1.4×10^{-8} $m^2 V^{-1} s^{-1}$ in the blend. The origin of this strong increase is not yet clear; It has been shown that films of MDMO-PPV exhibit interconnected ringlike features, due to asymmetric side chains.[81] This seems to be consistent with the proposition made by Pacios et al.,[82] who propose that the change in film morphology upon adding PCBM molecules results in an enhanced intermolecular interaction and, therefore, in an improved charge transfer between adjacent polymer chains. Based on this consideration, an enhancement in hole transport is possible. For fullerene concentration larger than 67 wt % the hole mobility saturates. It has been pointed out by van Duren et al. that phase separation, resulting in pure PCBM domains surrounded by a homogeneous matrix of 50:50 wt % MDMO-PPV:PCBM, sets in for concentrations of more than 67 wt % PCBM.[79] As a result, the hole mobility in this homogeneous matrix of 50:50 PPV:PCBM is indeed expected to saturate, as is observed experimentally (Fig. 5). For PPV derivatives with symmetrical side-chains, it has been observed that instead of ringlike structures, more rodlike features are formed. It is known that PPV derivatives with symmetrical side chains exhibit an enhanced mobility due to a reduction of the disorder. In Figure 6 the hole mobility in the random symmetric co-polymer poly[2,5-bis(2-ethylhexyloxy)-*co*-2,5-bis(2-methylbutyloxy)-1,4-phenylene vinylene] (BEH_1BMB_3-PPV) (see inset) is shown for a number of PCBM fractions. In contrast to MDMO-PPV, the mobility enhancement is only very weak, a factor of 4 instead of 400. This dependence of the mobility enhancement on the chemical structure of the PPV derivative suggests that PCBM changes the packing of the MDMO-PPV.

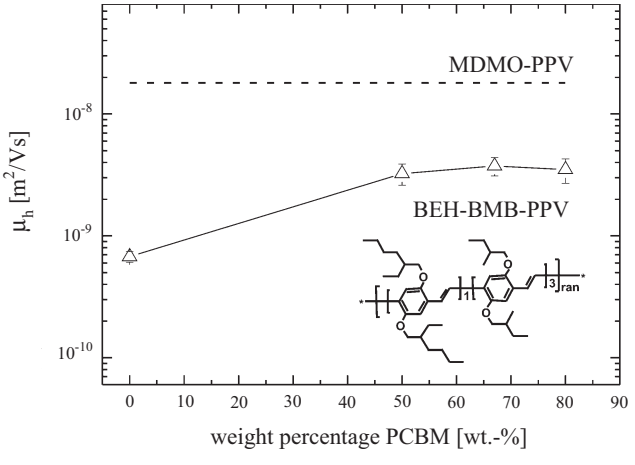

Figure 6. Hole zero-field mobility μ_h in blends of BEH_1BMB_3-PPV, shown in the inset, for various PCBM weight percentages (symbols), at room temperature (295 K). The mobilities were calculated from the SCL currents. Also the mobility achieved in MDMO-PPV for >80 wt % PCBM is indicated (dashed line).

2.5. Extraction of the Charge Carriers at the Electrodes

In addition to attempts to optimize the components and composition of the active layer, modification of the electrodes has also lead to an improvement in device performance.[83–85] It is evident that the work function of the negatively charged electrode is relevant for the open-circuit voltage (V_{OC}) of the cells. In the classical metal–insulator–metal (MIM) concept, the V_{OC} is in first order approximation governed by the work function difference of the anode and the cathode, respectively. It should be noted that this only holds for the case where the Fermi levels of the contacts are within the bandgap of the insulator and are sufficiently far away from the HOMO and the lowest unoccupied molecular orbital (LUMO) levels, respectively. In the case of ohmic contacts, meaning that the negative and positive electrodes match the LUMO level of the acceptor and the HOMO level of the donor, respectively, the situation is different; charge transfer of electrons or holes from the metal into the semiconductor occurs in order to align the Fermi level at the negative and positive electrode, respectively. As a result, the electrode work functions become pinned close to the LUMO/HOMO level of the semiconductor.[84] Because of this pinning, the V_{OC} will be governed by the energetics of the LUMO of the acceptor and the HOMO of the donor. Indeed, in BHJ solar cells, a linear correlation of the V_{OC} with the reduction potential of the acceptor has been reported.[83] The fact that a slope unity was obtained indicates a strong coupling of the V_{OC} to the reduction strength of the acceptors. Remarkably, the presence of the coupling between the V_{OC} and the reduction potential of the PCBM has been interpreted as proof against the MIM concept, although it is in full agreement with a MIM device with two ohmic contacts.

In contrast, only a very weak variation of the V_{OC} (160 meV) has been observed when varying the work function of the negative electrode from 5.1 eV (Au) to 2.9 eV (Ca).[83] This has been explained by pinning of the electrode Fermi level to the reduction potential of the fullerene. However, it has been pointed out that when the metal work function is reduced to such an extent that it is below the LUMO, the electrode work function will remain pinned close to the LUMO level of the semiconductor.[84] This explains why the V_{OC} only increases slightly when going from Al (4.2 eV) to Ca (2.9 eV), because the Ca work function will be pinned to the LUMO of the PCBM (3.7 eV). Furthermore, a variation of more than 0.5 V of the V_{OC} was observed when palladium was used as a top contact, ruling out Fermi level pinning because of the presence of a large amount of PCBM surface states.[84] At the anode side, electrochemical modification of the PEDOT work function showed a linear correlation with the V_{OC} of the MDMO:PCBM BHJ solar cells, as expected for a MIM like

device with non-ohmic contacts.[85] Recent results by Scharber et al. demonstrated a linear dependence of V_{OC} on the position of the HOMO level of the polymer, as expected for a MIM device with an ohmic hole contact.[86]

However, it has been observed that when employing Al as the top electrode, the insertion of LiF between organic layers and the metal not only enhances the V_{OC}, as expected from its work function, but also increases both the short-circuit current J_{SC} and fill factor *FF*.[87] The origin of this increase, and the resulting 20 % enhancement in the efficiency, is less clear. One explanation that has been proposed is that the insertion of a sub-nanometer LiF layer results in the formation of a better ohmic contact and consequent lowering of the series resistance of the device by a factor of three or four, which thereby increases the observed *FF*.[87] However, it must be stressed that in solar cells the top electrode *extracts* electrons from the device. A higher work function electrode will therefore not inhibit the electrons from leaving the active layer by an energy barrier. It is therefore expected that electrons are collected with equal efficiency whatever the electrode. On the other hand, the inclusion of an insulating layer between the metal and active layer results in a reduction in the collection efficiency and is less likely to be a factor when noble metals such as Ag, Au, and Pd are used as electrodes. Additionally, because the charge carrier generation process in the PPV/PCBM blend is not affected by the electrode, it is also not obvious why a change in the metal electrode would dramatically affect the series resistance. In Figure 7 the experimental photocurrent–voltage (J_L–V) characteristics of ITO/PEDOT:PSS/MDMO-PPV:PCBM/cathode (cathode = LiF/Al, Ag, Au, Pd) devices are shown. The V_{OC} values of these devices are: LiF/Al = 0.90 V; Ag = 0.70 V; Au = 0.59 V; Pd = 0.40 V.[88] The J_{SC} decreases from 28 A m^{-2} for LiF/Al to only 17 A m^{-2} for Pd. The same data are re-plotted in Figure 8, but now as a function of V_{OC}–V, which reflects the internal electric field in the device. It appears that all the individual curves coincide on one universal curve. This demonstrates that, as expected, the photogeneration processes in the photoactive layer are not dependent on the nature of the top electrode. Moreover, it shows that no additional contact resistance is induced when the top contact is changed from ohmic (LiF/Al) to non-ohmic (Ag, Au, Pd). This scaling with internal field provides valuable information regarding the operating mechanism of BHJ solar cells: First, it demonstrates that the photocurrents in these BHJ devices are field-driven, and that diffusion only plays a minor role. Secondly, the excellent scaling with the internal field also indicates that the electric field in these devices is approximately homogeneous. With a change of the top electrode, the V_{OC} is affected because of modification of the metal work function. The reason for the observed changes in J_{SC}, *FF*, and maximum power point (*MPP*) is now clear from Figure 8: the voltage area between the origin ($V = V_{OC}$) and the arrows ($V = 0$ V) reflect the active (fourth quadrant) part of the device for each top electrode. Consequently, a different region of the J_{ph}–($V_{OC} - V$) curve shown in Figure 8 is probed when V_{OC} is modified. The dependence of the photocurrent on the effective voltage ($V_{OC} - V$) or field in the device is thus responsible for the observed changes of J_{SC}, *FF*, and *MPP* when the top electrode is varied. In the next section the relevance of the dissociation and charge transport are evaluated with regard to the photocurrent generation and performance of solar cells based on PPV:PCBM blends.

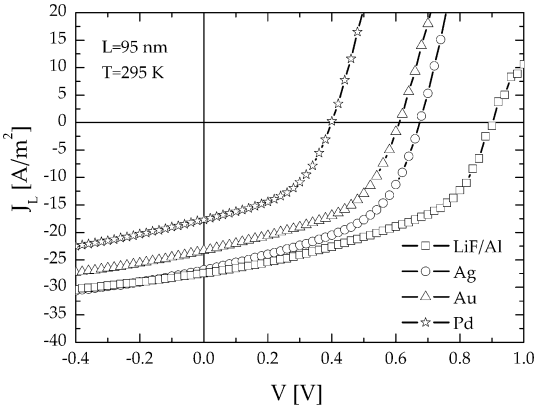

Figure 7. $J_L - V$ characteristics under illumination of an ITO/PEDOT:PSS/MDMO-PPV:PCBM 20:80 wt % photovoltaic devices, with LiF/Al, Ag, Au, and Pd as top electrodes (symbols). The devices were illuminated from a halogen lamp calibrated to an intensity of 800 W m^{-2}. The V_{OC} was found to be in the saturation regime in all cases. Reproduced with permission from [84]. Copyright 2003 American Institute of Physics.

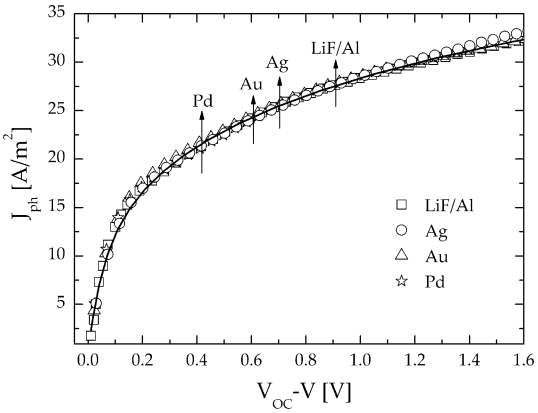

Figure 8. Photocurrent versus effective applied voltage ($V_{OC} - V$) of an MDMO-PPV:PCBM (20:80 wt %) device for four different top electrodes (symbols), at 295 K. The arrows indicate the short-circuit current densities ($V = 0$ V) and the corresponding open-circuit voltages of these devices. Reproduced with permission from [88]. Copyright 2004 American Institute of Physics.

3. Photocurrent Generation and Performance of Polymer:Fullerene Solar Cells

3.1. Modeling MDMO-PPV/PCBM (1:4 wt %) Bulk Heterojunction Solar Cells

A good understanding of the operation and processes limiting the performance of polymer:fullerene solar cells is crucial

for further optimization. The role of the contacts, drift, and diffusion of charge carriers, charge carrier generation, and recombination need to be clarified. The interpretation of current–voltage curves is often done by using models developed for inorganic p-n junctions.[89–92] However, in such a description, no detailed description of electric field distribution and carrier densities in BHJ solar cells has been given. Recently, Barker et al.[93] have presented a numerical model describing the current–voltage characteristics of bilayer conjugated polymer photovoltaic devices. In this model, the dissociation of bound electrons and holes at the donor acceptor interface was also included. However, because the electronic structures of bilayers and bulk heterojunctions are distinct, their operational principles are fundamentally different. In this section we establish the dependence of the photocurrent of bulk heterojunction MDMO-PPV:PCBM (1:4 wt %) devices on temperature and the applied voltage. Similar to the model of Barker, it is based on the standard set of the Poisson equation, current continuity equations, and current equations including both drift and diffusion.[94] The diffusion coefficients are obtained from the Einstein relation, but it should be noted that at high carrier densities the diffusion coefficient may be increased.[95] However, because the steady-state carrier densities are rather low in BHJ solar cells due to efficient extraction, we do not expect that this effect will play a large role. Furthermore, as pointed out in Section 2.3 the generation of free charge carriers from bound electron–hole pairs has been described by the geminate recombination theory of Onsager[56] in combination with a refinement proposed by Braun,[38] who pointed out the importance of the fact that the bound electron–hole pair has a finite lifetime. Finally, the recombination of free charge carriers is bimolecular, with a recombination strength given by the Langevin equation.[96] This numerical model describes the full current–voltage characteristics in the dark and under illumination, including the field-dependent generation rate $G(T,E)$. Figure 9 shows the effective photocurrent of a 120 nm thick MDMO-PPV/PCBM (20:80 wt %) BHJ solar cell (symbols) together with the numerical calculation (solid lines) for two different temperatures. At both temperatures, using the same parameters as presented above, the calculated photocurrent fits the experimentally data over the entire voltage range. For low effective voltages, $V_0 - V$, the photocurrent increases linearly with effective voltage due to a direct competition between diffusion and drift currents. At higher effective voltage, all free charge carriers are extracted for zero recombination, and the photocurrent saturates to $e\,G(T,E)\,L$. The two parameters governing the field- and temperature-dependent generation rate, the e–h pair distance a and the decay rate k_f, could be estimated by just equating the high-field photocurrents to $e\,G(E,T)\,L$, as shown in Figure 4. The numerical device model additionally includes the effects of space-charge and recombination. The values for the electron- and hole mobility used in these calculations are obtained experimentally (2×10^{-7} $m^2\,V^{-1}\,s^{-1}$ and 2×10^{-8} $m^2\,V^{-1}\,s^{-1}$, respectively).[69,75] Figure 9 indicates that

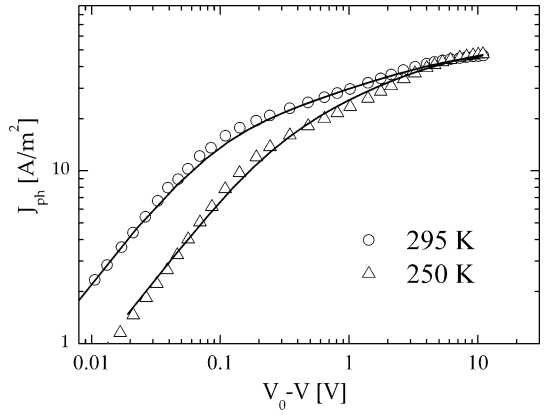

Figure 9. Effective photocurrent ($J_{ph}=J_L-J_D$) as a function of effective applied voltage (V_0-V) of MDMO-PPV:PCBM 20:80 device (symbols), at 295 and 250 K. The solid line represents the numerical calculation including diffusion, field dependent of generation rate $G(T,E)$ and recombination, for a device with a thickness of 120 nm.

the calculated photocurrent fits the experimental data over the entire voltage range. Under short-circuit conditions, the carrier densities and net generation rate are depicted in Figure 10. In the bulk of the device, the hole density is roughly one order of magnitude higher than the electron density. This

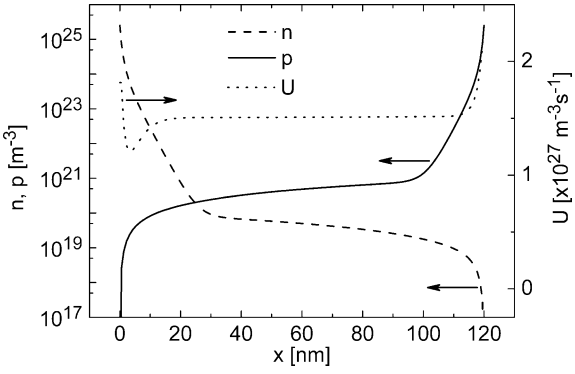

Figure 10. A 120 nm MDMO-PPV:PCBM (20:80 wt %) device at short circuit showing the carrier densities and the net generation rate.

is a result of the difference in mobility between electrons and holes. Since the holes are much slower, they accumulate in the device. However, with a mobility difference of only a factor of ten, the overall carrier densities are rather low as compared to other devices like LEDs or field-effect transistors (FETs). This is because the field in the device is quite large at SC and carriers are readily extracted. For this reason, space-charge effects only play a minor role, leading to a nearly constant field in the device.[94] This nearly constant field is consistent with the universal behavior of solar cells topped with various electrodes when scaled against the effective voltage across the device (Fig. 8). Furthermore, the model calculations revealed

that at short-circuit conditions only 7.0 % of the free charge carriers are lost due to bimolecular recombination and subsequent decay. This low loss of charge carriers is a consequence of the high field strength, which ensures good charge extraction, resulting in low carrier densities. Since the carrier densities are low, bimolecular recombination is weak and hence the recombination lifetime of the charge carriers is relatively long. Near the contacts, the bimolecular recombination rate R is especially low since one carrier is dominant (a consequence of the ohmic contacts). As a result, the net generation rate $U = G - R$ is highest at the contacts. As stated above, since the hole mobility is lower than the electron mobility, the bulk of the device is dominated by holes. Close to the cathode, but not in the immediate vicinity (about 5 nm), there still exists a considerable hole density, but here the electron density also strongly increases. Therefore, the rate of bimolecular recombination is enhanced close to the cathode, causing a dip in the net generation rate, as seen in Figure 10.

Furthermore, because of the high field strength, the time needed for the charge carriers to exit the device is quite small, and therefore, only few charge carriers are lost. We note that we have used a constant generation profile in the model calculations, whereas in BHJ solar cells, optical interference effects also play a role.[97] However, we verified that a spatial dependence of G does not affect the results presented here, as expected for a solar cell with only minor (bi)molecular recombination losses.

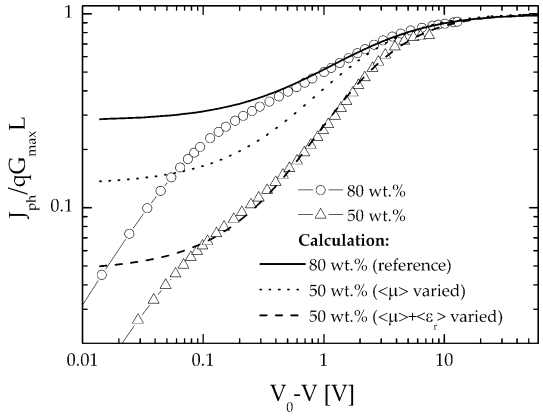

Figure 11. Experimental photocurrent (J_{ph}) normalized to its saturation value ($q\,G_{max}\,L$) as a function of effective applied voltage ($V_0 - V$) for two different MDMO-PPV:PCBM compositions (see legend). The lines represent the calculated dissociation probability of bound e–h pairs (P) at the donor/acceptor interface as follows: The solid line represents the calculated P that best fits the experimental data, with 80 wt % PCBM used as a reference. The dotted line denotes the calculated P for 50 wt % PCBM when only the charge-carrier mobilities have been modified; the dashed line represents the same calculation for the case when both mobility and the bulk dielectric constant are modified [78].

3.2. Effect of the PCBM Weight Fraction on the Solar-Cell Performance

In the MDMO-PPV:PCBM blends, the light is mainly absorbed in the PPV phase, and the role of PCBM is that of the electron acceptor and electron transport material. However, in order to obtain the maximum device efficiency up to 80 wt % PCBM has to be added to the PPV:PCBM mixture. Because the PCBM percolation limit is expected at only 17 vol %,[98,99] and the conjugated polymers even shows percolation at much lower fraction,[100] it is not obvious why it is necessary to add 80 wt % of a material that hardly contributes to the light absorption to obtain optimum performance. As shown in Figure 5, the hole mobility when going from 40 to 80 wt % PCBM increases by more than two orders of magnitude from the pure polymer to the blend (5×10^{-11} m^2 V^{-1} s^{-1} to ca. 1.4×10^{-8} m^2 V^{-1} s^{-1}). Furthermore, in the saturation regime $V_0 \times V > 0.1$ V the photocurrent is basically given by $J_{ph} = e\,G_{max}\,P(E,T)\,L$. In order to investigate the effect of the PCBM weight fraction on the dissociation efficiency $P(E,T)$, the measured photocurrents have been normalized to their saturation value ($q\,G_{max}\,L$), as shown in Figure 11 for the 50 and 80 wt % PCBM devices. This normalized photocurrent then reflects the dissociation efficiency in the saturation regime for effective voltages $V_0 \times V > 0.1$ V. It appears that a decrease of the PCBM weight fraction from 80 to 50 wt % leads to a strong reduction of the dissociation efficiency in the relevant voltage regime ($V_0 - V < 0.9$ V). The origin of this decrease in the dissociation efficiency of bound e–h pairs with decreasing PCBM concentration will be addressed by applying the device model discussed in Section 3.1: For low-mobility semiconductors, recombination of free carriers is given by the Langevin equation: $k_R = q\,\langle\mu\rangle/\varepsilon_0\langle\varepsilon_r\rangle$,with $\langle\varepsilon_r\rangle$ the spatially averaged dielectric constant of MDMO ($\varepsilon_r = 2.11$) and PCBM ($\varepsilon_r = 3.9$) (depending on their volume ratio) and $\langle\mu\rangle$ the effective charge carrier mobility of electrons and holes. The parameters in the model which vary with the PCBM fraction are k_F, ε_r, and k_R. Because the average dielectric constant and the charge carrier mobilities are known at each composition (Fig. 5), k_F remains the only adjustable parameter in our calculation when changing the composition. The dissociation efficiency of the device with 80 wt % PCBM (Fig. 4, solid line) will be used as a reference. From this calculation, a lifetime (k_F^{-1})of typically 2.5 μs was obtained. This long lifetime is in agreement with absorption spectroscopy measurements were bound e–h pairs in PPV:PCBM blends can still be detected after microseconds and even milliseconds, depending on temperature.[65,66] However, a quantitative comparison between our calculated k_F^{-1} of 2.5 μs and these transient absorption measurements is difficult because these measurements are performed at higher light intensity, charge density, and in the absence of an electric field. As a next step we systematically calculate $P(E,T)$ for a device with 50 wt % PCBM, changing the input parameters of the 80 wt % device one by one. First, we only adapt the charge carrier mobilities and take all other parameters as constant. It is observed from Figure 11 (dotted line) that the decrease of the electron-

and hole mobility, although dropping by approximately an order of magnitude from 80 to 50 wt % PCBM (Fig. 5), is not solely responsible for the observed decrease in dissociation efficiency. Subsequently, besides the mobility, the change in the spatially averaged dielectric constant $<\varepsilon_r>$, in accordance with the change in PPV and PCBM volume ratio, is also taken into account (dashed line). In this case, the calculated $P(E,T)$ exactly fits the experimental data without having to change any of the other parameters. Thus, the lower separation efficiency at 50 wt % PCBM results from the combination of a decreased charge-carrier mobility and lower dielectric constant, resulting in a stronger e–h binding energy. This result demonstrates that the mobilities, maximum generation rate, and spatially averaged dielectric constant are the key parameters which govern the composition dependence of the performance of OC_1C_{10}-PPV:PCBM based solar cells.

3.3. Formation of Space-Charges in PPV:PCBM Bulk Heterojunction Solar Cells

The external photocurrent becomes saturated when all photogenerated free electrons and holes are extracted from the semiconductor. This implies that the mean electron and hole drift lengths $w_{e(h)} = \mu_{e(h)} \tau_{e(h)} E$ are equal or longer than the specimen thickness L; where $\mu_{e(h)}$ is the charge-carrier mobility of electrons (holes), $\tau_{e(h)}$ is the charge-carrier lifetime, and E is the internal electric field. In this case, no recombination occurs and the saturated photocurrent density is simply given by $J_{ph}^{sat} = q\,G\,L$ with G the generation rate of free electrons and holes and q the electric charge. However, if either $w_e < L$, $w_h < L$, or both are smaller than L, space charge will form and recombination of free charge-carriers becomes significant. In other words, recombination becomes important when the transit time of the photogenerated free charge carriers is longer than their lifetime. Suppose now that the electron–hole pairs are photogenerated uniformly throughout the specimen and that the charge transport is strongly unbalanced, meaning that $w_e \neq w_h$. In the case that the recombination of free charge-carriers is bimolecular, the free electron- and hole lifetime are equal $\tau_e = \tau_h$. Then, a difference in w_e and w_h would originate from a difference in charge carrier mobility μ_e and μ_h. In an MDMO-PPV:PCBM blend with $\mu_h \ll \mu_e$ and $w_h < L$, the holes will accumulate to a greater extend in the device than the electrons, which makes the applied field nonuniform. As a consequence, the electric field increases in the region (L_1) near the anode, enhancing the extraction of holes. Conversely, in the region near the cathode the electric field decreases, diminishing the extraction of electrons. It is evident that in the region L_1 the accumulated holes are not neutralized by an equal density of electrons, which results in a build-up of positive space-charge. Goodman and Rose pointed out that that there is a fundamental limit to be expected for the built-up of space charge in a semiconductor at high light-intensities; The electrostatic limit of hole accumulation is reached when the photocurrent generated in this region, $J_{ph} = q\,G\,L_1$, is equal to the SCLC[63]

$$J_{SCL} = \frac{9}{8}\varepsilon_0\varepsilon_r\mu_h\frac{V_1}{L_1} \tag{6}$$

where $\varepsilon_0\,\varepsilon_r$ is the dielectric permittivity. By equating $q\,G\,L_1$ with Equation 6 it follows that the length of the region L_1 in this space-charge-limited regime is given by

$$L_1 = (9/8\varepsilon_0\varepsilon_r\mu_h/8qG)^{1/4}V^{1/2} \tag{7}$$

Because $V_1 \approx V$, the maximum electrostatically allowed photocurrent that can be extracted from the device is[63]

$$J_{ph} = q\left(\frac{9\varepsilon_0\varepsilon_r\mu_h}{8q}\right)^{1/4}G^{3/4}V^{1/2} \tag{8}$$

The SCL photocurrent scales with a 3/4 power dependence on light intensity (Eq. 8), whereas in the absence of space-charge limitations the photocurrent is expected to scale linearly with the light intensity. The occurrence of a space-charge limit in solar cells based on amorphous Si has also been discussed by Crandall[101,102] and more recently by Schiff.[103] As shown in Section 2.4, in MDMO-PPV:PCBM blends the hole mobility in the blend is enhanced by a factor of 400 as compare with the pure material, resulting in a much more balanced transport. The remaining mobility difference of only one order of magnitude is not sufficient to induce SCL photocurrents. This is confirmed by the fact that for MDMO-PPV:PCBM cells the photocurrent closely follows linear behavior with light intensity.[79,104] As demonstrated in Section 2.4, when symmetrical substituted PPV is used (such as BEH_1BMB_3-PPV), the hole mobility in the polymer phase is hardly affected by the presence of PCBM, resulting in an increased mobility difference between electrons and holes in the blend. At room temperature the electron mobility in the PCBM phase ($\mu_e = 4 \times 10^{-7}$ $m^2\,V^{-1}\,s^{-1}$) is a factor of 125 larger than hole mobility in the BEH_1BMB_3-PPV phase ($\mu_h = 3.2 \times 10^{-9}$ $m^2\,V^{-1}\,s^{-1}$). This difference further increases to a factor of 2000 at T = 210 K because of the difference in activation energy between the electron- (0.18 eV) and hole mobility (0.35 eV). Figure 12 shows the experimental J_{ph} as a function of $V_0 - V$ in a 20:80 blend of BEH_1BMB_3-PPV:PCBM at 210 K for different light-intensities. It is observed that for $V_0 - V < 0.06$ V, the J_{ph} shows linear dependence on voltage. However, above 0.06 V the experimental J_{ph} clearly shows a square-root dependence on voltage, as is predicted by Equation 8 for very different μ_e and μ_h values. At larger voltages J_{ph} shows a clear transition to the saturation regime, where it becomes limited by the field- and temperature dependence of the generation rate $G(E,T)$. The incident light power (ILP) was varied from 80 mW cm^{-2} (upper curve) down to 6 mW cm^{-2} using a set of neutral density filters. It appears from Figure 12 that the J_{ph} shows weaker light intensity dependence at low voltages in the square-root regime, than at high voltages in the saturation regime. Figure 13a shows, in a double logarithmic plot, the experimental J_{ph} taken from Fig-

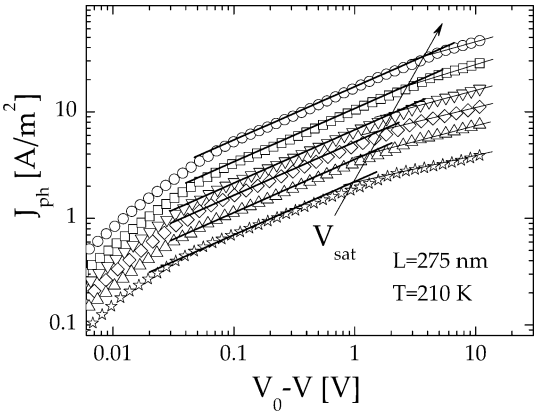

Figure 12. Incident light power (*ILP*) dependence of the photocurrent (J_{ph}) versus the effective voltage ($V_0 - V$) measured at $T = 210$ K. The solid (thick) line represents the calculated J_{ph} from Equation 8 using $\mu_h = 1.2 \times 10^{-11}$ $m^2 V^{-1} s^{-1}$, $\varepsilon_r = 2.6$, and $G \approx ILP$, where *ILP* was varied from 80 to 6 mW cm^{-2}. The arrow indicates the voltage (V_{sat}) at which J_{ph} shows the transition to the saturation regime [105].

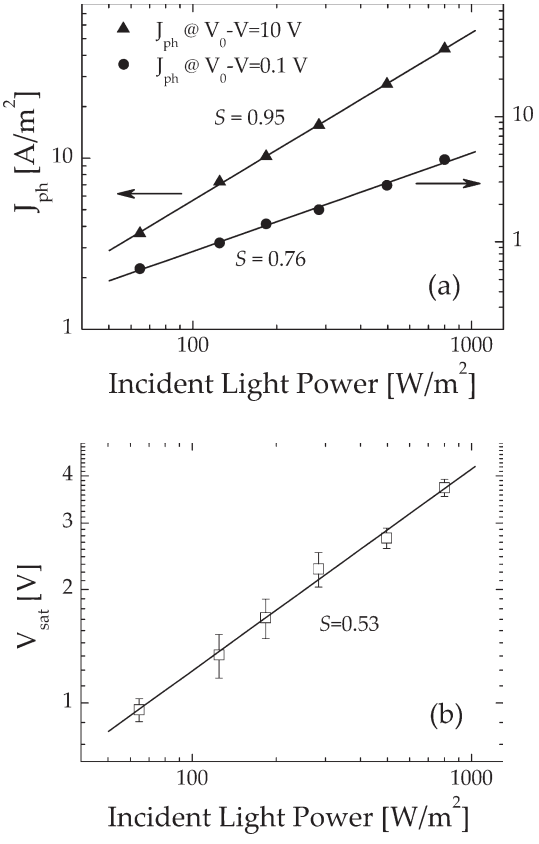

Figure 13. a) *ILP* dependence of the photocurrent J_{ph} taken from Figure 11 at an effective voltage of $V_0 - V = 0.1$ V and $V_0 - V = 10$ V (symbols). b) Saturation voltage (V_{sat}) versus *ILP* as determined for Figure 11. The slope (*S*) determined from the linear fit (solid lines) to the experimental data is written on the figure. Reproduced with permission from [105]. Copyright 2005 American Physical Society.

ure 11 as a function of *ILP* for two different voltages, at $V_0 - V = 0.1$ V in the square-root regime and at $V_0 - V = 10$ V in the saturation regime. The slope *S* determined from the linear fit (solid lines) to the experimental data amounts to $S = 0.76$ in the square-root part and $S = 0.95$ in the saturation part at high voltages. The 1/2 power dependence of J_{ph} on voltage and 3/4 dependence on *ILP* is a strong indication for the occurrence of a space-charge-limited photocurrent in this materials system.

Another way to confirm the presence of a SCL photocurrent is to consider the voltage V_{sat} at which J_{ph} switches from the square-root dependence to the saturation regime. This transition occurs when the hole-accumulation region (L_1) becomes equal to the device thickness. In case of a SCL photocurrent V_{sat} scales with the square-root of *G*. In contrast, in the absence of a space-charge limit (Eq. 1) the transition voltage will be independent of light intensity.[57] In Figure 12, the voltage V_{sat} at which the transition occurs is determined from the crossover point of the square-root dependence and the extrapolated saturation part, as indicated by the arrow. In Figure 12, it is already evident that V_{sat} shows a clear variation with light intensity. In Figure 13b, V_{sat} is plotted in double logarithmic scale as a function of *ILP*. A slope $S = 0.51$ is found, in agreement with the space-charge-limited prediction. This is further conformation that the photocurrent in 20:80 blends of BEH_1BMB_3-PPV:PCBM devices is truly limited by space-charge effects. This space-charge-limited photocurrent is the maximum electrostatically allowed current that can be generated into the external circuit of any solar cell. Furthermore, a J_{ph} limited by space charges also has an impact on the power conversion efficiency of solar cells. Because the J_{ph} is governed by a square-root dependence on voltage (Fig. 12), the fill factors of space-charge-limited solar cells are typically limited to only ca. 42 %.

4. Outlook

Recently, polymer/fullerene BHJs, based on P3HT as donor and PCBM as acceptor have reached power conversion efficiencies of 3.5 %.[96] Although further improvement of device fabrication has lead to efficiencies of over 4 % for this material combination,[97,98] efficiencies are not yet high enough for commercial application. As the incident photon to collected electron efficiency (IPCE) is already high, up to 70 % at the absorption maximum of P3HT, it is unclear how much and in what way the efficiency of these devices can be further improved. As a first approximation Coakley and McGehee predicted that an efficiency of 10 % may be within reach.[106] In their calculation it is assumed, among other things, that the fill factor is equal to unity, and recombination, either geminate or bimolecular, is neglected. Our ability to accurately model the photocurrent–voltage characteristics of polymer/fullerene solar cells enables us to perform a more detailed calculation. By combining charge carrier mobility measurements with current–voltage measurements performed on illuminated solar cells, we quantitatively model the experimental current–voltage characteristics of P3HT:PCBM solar cells. The obtained

theoretical description of P3HT/PCBM solar cells enables us to investigate the enhancement of the efficiency when a number of solar-cell parameters are varied. We focused on two effects: First the effect of minimizing the energy loss in the electron transfer from donor to acceptor material was found to be of paramount importance; an efficiency of 8.4 % is predicted.[107] This efficiency increase stems from an increase of V_{OC}. Subsequently, the effect of lowering the polymeric bandgap is studied. Several research groups have put a lot of effort in the synthesis and application of these polymers. At first glance, a low bandgap polymer seems beneficial. As a result of enhanced overlap with the solar-cell spectrum the absorption is enhanced, leading to efficiencies larger than 6 %. Surprisingly, the model calculations show that once the energy loss in electron transfer is minimized, the best performing solar cell comprises a polymer with a bandgap of around 2 eV, clearly not a low bandgap. In the BHJ cells, a lowering of the bandgap is accompanied by a decrease of the open-circuit voltage, canceling the benefit of an absorption increase. Ultimately, with energy levels, bandgaps, and mobilities simultaneously optimized, single-layer polymer/fullerene solar cells can reach nearly 11 % efficiency.[107] In order to reach efficiencies beyond 11 %, tandem cells, consisting of multiple layers each with their specific absorption maximum and width, should be realized. Although multiple-layer tandem cells seem incompatible with processing from solution, the first working tandem cell based on spin-coated BHJ solar cells with different absorption spectra has recently been realized.[108]

Received: May 19, 2006
Revised: September 25, 2006
Published online: May 23, 2007

[1] D. M. Chapin, C. S. Fuller, G. L. Pearson, *J. Appl. Phys.* **1954**, *25*, 676.
[2] M. A. Green, K. Emery, D. L. King, S. Igari, W. Warta, *Prog. Photovoltaics* **2005**, *13*, 49.
[3] W. Shockley, H. J. Queisser, *J. Appl. Phys.* **1961**, *32*, 510.
[4] M. A. Green, *Solar Cells: Operating Principles, Technology and System Applications*, Prentice-Hall, Englewood Cliffs, NJ, **1982**.
[5] S. E. Shaheen, R. Radspinner, N. Peyghambarian, G. E. Jabbour, *Appl. Phys. Lett.* **2001**, *79*, 2996.
[6] G. Gustafsson, Y. Cao, G. M. Treacy, F. Klavetter, N. Colaneri, A. J. Heeger, *Nature* **1992**, *357*, 477.
[7] H. Kallmann, M. Pope, *J. Chem. Phys.* **1959**, *30*, 585.
[8] S. Barth, H. Bässler, *Phys. Rev. Lett.* **1997**, *79*, 4445.
[9] P. G. Dacosta, E. M. Conwell, *Phys. Rev. B* **1993**, *48*, 1993.
[10] R. N. Marks, J. J. M. Halls, D. D. C. Bradley, R. H. Friend, A. B. Holmes, *J. Phys. Condens. Matter* **1994**, *6*, 1379.
[11] V. Choong, Y. Park, Y. Gao, T. Wehrmeister, K. Mullen, B. R. Hsieh, C. W. Tang, *Appl. Phys. Lett.* **1996**, *69*, 1492.
[12] J. J. M. Halls, K. Pichler, R. H. Friend, S. C. Moratti, A. B. Holmes, *Appl. Phys. Lett.* **1996**, *68*, 3120.
[13] J. J. M. Halls, R. H. Friend, *Synth. Met.* **1997**, *85*, 1307.
[14] D. E. Markov, E. Amsterdam, P. W. M. Blom, A. B. Sieval, J. C. Hummelen, *J. Phys. Chem. A* **2005**, *109*, 5266.
[15] D. E. Markov, C. Tanase, P. W. M. Blom, J. Wildeman, *Phys. Rev. B* **2005**, *72*, 045 217.
[16] C. W. Tang, *Appl. Phys. Lett.* **1986**, *48*, 183.
[17] M. Grätzel, *Nature* **2001**, *414*, 338.
[18] B. O'Regan, M. Grätzel, *Nature* **1991**, *353*, 737.
[19] A. K. Jana, *J. Photochem. Photobiol. A* **2000**, *132*, 1.
[20] P. Peumans, V. Bulovic, S. R. Forrest, *Appl. Phys. Lett.* **2000**, *76*, 2650.
[21] B. A. Gregg, *Chem. Phys. Lett.* **1996**, *258*, 376.
[22] M. Granstrom, K. Petritsch, A. C. Arias, A. Lux, M. R. Andersson, R. H. Friend, *Nature* **1998**, *395*, 257.
[23] J. J. M. Halls, C. A. Walsh, N. C. Greenham, E. A. Marseglia, R. H. Friend, S. C. Moratti, A. B. Holmes, *Nature* **1995**, *376*, 498.
[24] G. Yu, J. Gao, J. C. Hummelen, F. Wudl, A. J. Heeger, *Science* **1995**, *270*, 1789.
[25] C. J. Brabec, N. S. Sariciftci, J. C. Hummelen, *Adv. Funct. Mater.* **2001**, *11*, 15.
[26] S. Morita, A. A. Zakhidov, K. Yoshino, *Solid State Commun.* **1992**, *82*, 249.
[27] N. S. Sariciftci, L. Smilowitz, A. J. Heeger, F. Wudl, *Science* **1992**, *258*, 1474.
[28] S. E. Shaheen, C. J. Brabec, N. S. Sariciftci, F. Padinger, T. Fromherz, J. C. Hummelen, *Appl. Phys. Lett.* **2001**, *78*, 841.
[29] D. Chirvase, J. Parisi, J. C. Hummelen, V. Dyakonov, *Nanotechnology* **2004**, *15*, 1317.
[30] Y. Kim, S. A. Choulis, J. Nelson, D. D. C. Bradley, S. Cook, J. R. Durrant, *Appl. Phys. Lett.* **2005**, *86*, 063 502.
[31] F. Padinger, R. S. Rittberger, N. S. Sariciftci, *Adv. Funct. Mater.* **2003**, *13*, 85.
[32] C. J. Brabec, *Sol. Energy Mater. Sol. Cells* **2004**, *83*, 273.
[33] X. Yang, J. Loos, S. C. Veenstra, W. J. H. Verhees, M. M. Wienk, J. M. Kroon, M. A. J. Michels, R. A. J. Janssen, *Nano Lett.* **2005**, *5*, 579.
[34] G. Li, V. Shrotriya, J. Huang, Y. Yao, T. Moriarty, K. Emery, Y. Yang, *Nat. Mater.* **2005**, *4*, 864.
[35] W. Ma, C. Yang, X. Gong, K. Lee, A. J. Heeger, *Adv. Funct. Mater.* **2005**, *15*, 1617.
[36] M. Reyes-Reyes, K. Kim, D. L. Carroll, *Appl. Phys. Lett.* **2005**, *87*, 083 506.
[37] C. J. Brabec, G. Zerza, G. Cerullo, S. De Silvestri, S. Luzzati, J. C. Hummelen, S. Sariciftci, *Chem. Phys. Lett.* **2001**, *340*, 232.
[38] C. L. Braun, *J. Chem. Phys.* **1984**, *80*, 4157.
[39] T. E. Goliber, J. H. Perlstein, *J. Chem. Phys.* **1984**, *80*, 4162.
[40] K. Pakbaz, C. H. Lee, A. J. Heeger, T. W. Hagler, D. McBranch, *Synth. Met.* **1994**, *64*, 295.
[41] U. Albrecht, H. Bässler, *Chem. Phys.* **1995**, *199*, 207.
[42] M. Deussen, M. Scheidler, H. Bässler, *Synth. Met.* **1995**, *73*, 123.
[43] R. Kersting, U. Lemmer, M. Deussen, H. J. Bakker, R. F. Mahrt, H. Kurz, V. I. Arkhipov, H. Bässler, E. O. Göbel, *Phys. Rev. Lett.* **1994**, *73*, 1440.
[44] G. Yu, A. J. Heeger, *J. Appl. Phys.* **1995**, *78*, 4510.
[45] M. Theander, A. Yartsev, D. Zigmantas, V. Sundstrom, W. Mammo, M. R. Andersson, O. Inganas, *Phys. Rev. B* **2000**, *61*, 12 957.
[46] A. Haugeneder, M. Neges, C. Kallinger, W. Spirkl, U. Lemmer, J. Feldmann, U. Scherf, E. Harth, A. Gugel, K. Mullen, *Phys. Rev. B* **1999**, *59*, 15 346.
[47] T. Stubinger, W. Brutting, *J. Appl. Phys.* **2001**, *90*, 3632.
[48] T. J. Savenije, J. M. Warman, A. Goossens, *Chem. Phys. Lett.* **1998**, *287*, 148.
[49] C. Schlebusch, B. Kessler, S. Cramm, W. Eberhardt, *Synth. Met.* **1996**, *77*, 151.
[50] T. I. Hukka, T. Toivonen, E. Hennebicq, J.-L. Brédas, R. A. J. Janssen, D. Beljonne, *Adv. Mater.* **2006**, *18*, 1301
[51] Y. Liu, M. A. Summers, S. R. Scully, M. D. McGehee, *J. Appl. Phys.* **2006**, *99*, 093 521.
[52] P. M. Borsenberger, D. S. Weiss, *Organic Photoreceptors for Xerography*, Marcel Dekker, New York **1998**.
[53] P. M. Borsenberger, L. E. Contois, D. C. Hoesterey, *J. Chem. Phys.* **1978**, *68*, 637.
[54] P. M. Borsenberger, A. I. Ateya, *J. Appl. Phys.* **1978**, *49*, 4035.

[55] R. R. Chance, C. L. Braun, *J. Chem. Phys.* **1976**, *64*, 3573.
[56] L. Onsager, *Phys. Rev.* **1938**, *54*, 554.
[57] D. Hertel, E. V. Soh, H. Bässler, L. J. Rothberg, *Chem. Phys. Lett.* **2002**, *361*, 99.
[58] J. Nelson, *Phys. Rev. B* **2003**, *67*, 155209.
[59] P. Peumans, S. R. Forrest, *Chem. Phys. Lett.* **2004**, *398*, 27.
[60] T. Offermans, S. C. J. Meskers, R. A. J. Janssen, *Chem. Phys.* **2005**, *308*, 125.
[61] V. I. Arkhipov, P. Heremans, H. Bässler, *Appl. Phys. Lett.* **2003**, *82*, 4605.
[62] J. G. Müller, J. M. Lupton, J. Feldmann, U. Lemmer, M. C. Scharber, N. S. Sariciftci, C. J. Brabec, U. Scherf, *Phys. Rev. B* **2005**, *72*, 195208.
[63] A. M. Goodman, A. Rose, *J. Appl. Phys.* **1971**, *42*, 2823.
[64] A. F. Nogueira, I. Montanari, J. Nelson, J. R. Durrant, C. Winder, N. S. Sariciftci, C. Brabec, *J. Phys. Chem. B* **2003**, *107*, 1567.
[65] I. Montanari, A. F. Nogueira, J. Nelson, J. R. Durrant, C. Winder, M. A. Loi, N. S. Sariciftci, C. J. Brabec, *Appl. Phys. Lett.* **2002**, *81*, 3001.
[66] T. Offermans, S. C. J. Mesker, R. A. J. Janssen, *J. Chem. Phys.* **2003**, *119*, 10924.
[67] R. Sokel, R. C. Hughes, *J. Appl. Phys.* **1982**, *53*, 7414.
[68] V. D. Mihailetchi, L. J. A. Koster, J. C. Hummelen, P. W. M. Blom, *Phys. Rev. Lett.* **2004**, *93*, 216601.
[69] V. D. Mihailetchi, J. K. J. van Duren, P. W. M. Blom, J. C. Hummelen, R. A. J. Janssen, J. M. Kroon, M. T. Rispens, W. J. H. Verhees, M. M. Wienk, *Adv. Funct. Mater.* **2003**, *13*, 43.
[70] P. W. M. Blom, M. J. M. de Jong, M. G. van Munster, *Phys. Rev. B* **1997**, *55*, R656.
[71] W. Geens, S. E. Shaheen, C. J. Brabec, J. Poortmans, N. S. Sariciftci, *AIP Conf. Proc.* **2000**, *544*, 516.
[72] C. Tanase, E. J. Meijer, P. W. M. Blom, D. M. de Leeuw, *Phys. Rev. Lett.* **2003**, *91*, 216601.
[73] S. A. Choulis, J. Nelson, Y. Kim, D. Poplavskyy, T. Kreouzis, J. R. Durrant, D. D. C. Bradley, *Appl. Phys. Lett.* **2003**, *83*, 3812.
[74] R. Pacios, J. Nelson, D. D. C. Bradley, C. J. Brabec, *Appl. Phys. Lett.* **2003**, *83*, 4764.
[75] C. Melzer, E. Koop, V. D. Mihailetchi, P. W. M. Blom, *Adv. Funct. Mater.* **2004**, *14*, 865.
[76] I. H. Campbell, S. Rubin, T. A. Zawodzinski, J. D. Kress, R. L. Martin, D. L. Smith, N. N. Barashkov, J. P. Ferraris, *Phys. Rev. B* **1996**, *54*, 14321.
[77] B. de Boer, A. Hadipour, M. M. Mandoc, T. Van Woudenbergh, P. W. M. Blom, *Adv. Mater.* **2005**, *17*, 621.
[78] V. D. Mihailetchi, L. J. A. Koster, P. W. M. Blom, C. Melzer, B. de Boer, J. K. J. van Duren, R. A. J. Janssen, *Adv. Funct. Mater.* **2005**, *15*, 795.
[79] J. K. J. van Duren, X. Yang, J. Loos, C. W. T. Bulle-Lieuwma, A. B. Sieval, J. C. Hummelen, R. A. J. Janssen, *Adv. Funct. Mater.* **2004**, *14*, 425.
[80] S. M. Tuladhar, D. Poplavskyy, S. A. Choulis, J. R. Durrant, D. D. C. Bradley, J. Nelson, *Adv. Funct. Mater.* **2005**, *15*, 1171.
[81] M. Kemerink, J. K. J. van Duren, P. Jonkheijm, W. F. Pasveer, P. M. Koenraad, R. A. J. Janssen, H. W. M. Salemink, J. H. Wolter, *Nano Lett.* **2003**, *3*, 1191.
[82] R. Pacios, D. D. C. Bradley, J. Nelson, C. J. Brabec, *Synth. Met.* **2003**, *137*, 1469.
[83] C. J. Brabec, A. Cravino, D. Meissner, N. S. Sariciftci, T. Fromherz, M. T. Rispens, L. Sanchez, J. C. Hummelen, *Adv. Funct. Mater.* **2001**, *11*, 374.
[84] V. D. Mihailetchi, P. W. M. Blom, J. C. Hummelen, M. T. Rispens, *J. Appl. Phys.* **2003**, *94*, 6849.
[85] H. Frohne, S. E. Shaheen, C. J. Brabec, D. C. Muller, N. S. Sariciftci, K. Meerholz, *ChemPhysChem* **2002**, *3*, 795.
[86] M. C. Scharber, D. Mühlbacher, M. Koppe, P. Denk, C. Waldauf, A. J. Heeger, C. Brabec, *Adv. Mater.* **2006**, *18*, 789.
[87] C. J. Brabec, S. E. Shaheen, C. Winder, N. S. Sariciftci, *Appl. Phys. Lett.* **2002**, *80*, 1288.
[88] V. D. Mihailetchi, L. J. A. Koster, P. W. M. Blom, *Appl. Phys. Lett.* **2004**, *85*, 970.
[89] E. A. Katz, D. Faiman, S. M. Tuladhar, J. M. Kroon, M. M. Wienk, T. Fromherz, F. Padinger, C. J. Brabec, N. S. Sariciftci, *J. Appl. Phys.* **2001**, *90*, 5343.
[90] V. Dyakonov, *Phys. E* **2002**, *14*, 53.
[91] C. J. Brabec, S. E. Shaheen, C. Winder, N. S. Sariciftci, P. Denk, *Appl. Phys. Lett.* **2002**, *80*, 1288.
[92] P. Schilinsky, C. Waldauf, J. Hauch, C. J. Brabec, *J. Appl. Phys.* **2004**, *95*, 2816.
[93] J. A. Barker, C. M. Ramsdale, N. C. Greenham, *Phys. Rev. B* **2003**, *67*, 075205.
[94] L. J. A. Koster, E. C. P. Smits, V. D. Mihailetchi, P. W. M. Blom, *Phys. Rev. B* **2005**, *72*, 085205.
[95] Y. Roichman, N. Tessler, *Appl. Phys. Lett.* **2002**, *80*, 1948.
[96] P. Langevin, *Ann. Chim. Phys.* **1903**, *28*, 433.
[97] H. Hoppe, N. Arnold, D. Meissner, N. S. Sariciftci, *Thin Solid Films* **2004**, *451*, 589.
[98] A. Aharony, D. Stauffer, *Introduction to Percolation Theory*, 2nd ed., Taylor and Francis, London **1993**.
[99] S. Hotta, S. D. D. V. Rughooputh, A. J. Heeger, *Synth. Met.* **1987**, *22*, 79.
[100] A. J. Heeger, *Trends Polym. Sci.* **1995**, *3*, 39.
[101] R. S. Crandall, *J. Appl. Phys.* **1984**, *55*, 4418
[102] R. S. Crandall, *J. Appl. Phys.* **1983**, *54*, 7176
[103] E. A. Schiff, *Sol. Eng. Mater. Sol. Cells* **2003**, *78*, 567.
[104] P. Schilinsky, C. Waldauf, C. J. Brabec, *Appl. Phys. Lett.* **2002**, *81*, 3885.
[105] V. D. Mihailetchi, J. Wildeman, P. W. M. Blom, *Phys. Rev. Lett.* **2005**, *94*, 126602.
[106] K. M. Coakley, M. D. McGehee, *Chem. Mater.* **2004**, *16*, 4533.
[107] L. J. A. Koster, V. D. Mihailetchi, P. W. M. Blom, *Appl. Phys. Lett.* **2006**, *88*, 093511.
[108] A. Hadipour, B. de Boer, J. Wildeman, F. B. Kooistra, J. C. Hummelen, M. G. R. Turbiez, M. M. Wienk, R. A. J. Janssen, P. W. M. Blom, *Adv. Funct. Mater.* **2006**, *16*, 1897.